Available online at www.sciencedirect.com
ScienceDirect
Biomaterials 29 (2008) 2548–2555
Biomaterials
www.elsevier.com/locate/biomaterials

Fluorescent magnetic nanohybrids as multimodal imaging agents for human epithelial cancer detection

Jaemoon Yang [a], Eun-Kyung Lim [a], Hong Jae Lee [b], Joseph Park [a], Sang Cheon Lee [b], Kwangyeol Lee [c], Ho-Geun Yoon [d], Jin-Suck Suh [e], Yong-Min Huh [e,**], Seungjoo Haam [a,*]

[a] *Department of Chemical Engineering, Yonsei University, 134 Shinchon-dong Seodaemoon-ku, Seoul 120-749, Republic of Korea*
[b] *Nanomaterials Application Division, Korea Institute of Ceramic Engineering and Technology, Seoul 153-801, Republic of Korea*
[c] *Department of Chemistry, Korea University, Seoul 136-701, Republic of Korea*
[d] *Department of Biochemistry and Molecular Biology, Yonsei University, Seoul 120-752, Republic of Korea*
[e] *Department of Radiology, College of Medicine, Yonsei University, Seoul 120-752, Republic of Korea*

Received 24 October 2007; accepted 28 December 2007
Available online 10 March 2008

Abstract

Cetuximab conjugated fluorescent magnetic nanohybrids (CET-FMNHs) were synthesized for detection of human epithelial cancer via magnetic resonance (MR) and optical imaging. Spherical FMNHs consist of $MnFe_2O_4$ magnetic nanocrystals encapsulated in pyrene-labeled PCL-*b*-PMAA as a surfactant prepared by a nano-emulsion method. FMNHs demonstrated excellent colloidal stability and biocompatibility for biomedical application. Antibody conjugated fluorescent magnetic nanohybrids (CET-FMNHs) served as effective agents for both magnetic resonance (MR) and fluorescence optical imaging of cancer cell lines.

Keywords: Magnetic nanoparticle; Fluorescence; Nanohybrid; Cancer; Cetuximab

1. Introduction

Magnetic nanoparticles have been extensively utilized for the noninvasive imaging of molecular markers for cancer detection, cell tracking, cell sorting, and cell sensing [1–6]. In particular, the utility of magnetic nanoparticles as an effective agent in magnetic resonance (MR) imaging has been extremely successful when measuring the morphology and function of healthy and diseased soft tissues *in vivo* [1,2,7]. The ultra-sensitive magnetic nanocrystals (MNCs) as MR probes have been developed for the detection of early state of cancer and lymph node [1,8]. Recent studies include the size effect, composition, and assemblies of MNCs for enhancing magnetic sensitivity under magnetic field [1,9].

Combination of magnetic and optical imaging into a nanostructured system would greatly benefit *in vivo* disease diagnosis as well as the *in situ* monitoring of living cells [10–12]. However, the synthetic procedure of previous works requires the multi-step chemical treatments in order to conjugate fluorescence dyes on the MNC surface and to improve the colloidal stability in an aqueous phase. In our work, thus, we suggested simple and stable fluorescent magnetic nanohybrids synthesis as multimodal imaging agents using nano-emulsion method for detection of cancer (Fig. 1).

As effective MR imaging probes, monodispersed and magnetically ultra-sensitive magnetic nanocrystals (MNCs) were synthesized in the organic phase [1–13]. However, these magnetic nanocrystals could not be applied to biomedical application without an appropriate surface modification to give required colloidal stability in the aqueous phase [14]. In order to prepare the waster-soluble magnetic compounds, we first synthesized the pyrene-labeled poly(ϵ-caprolactone)-*b*-poly(methacrylic acid) as a phase transfer agent [15]. By using

* Corresponding author. Tel.: +82 2 2123 2751; fax: +82 2 312 6401.
** Corresponding author. Tel.: +82 2 2228 2375; fax: 82 2 362 8647.
E-mail addresses: ymhuh@yuhs.ac (Y.-M. Huh), haam@yonsei.ac.kr (S. Haam).

0142-9612/$ - see front matter © 2008 Elsevier Ltd. All rights reserved.
doi:10.1016/j.biomaterials.2007.12.036

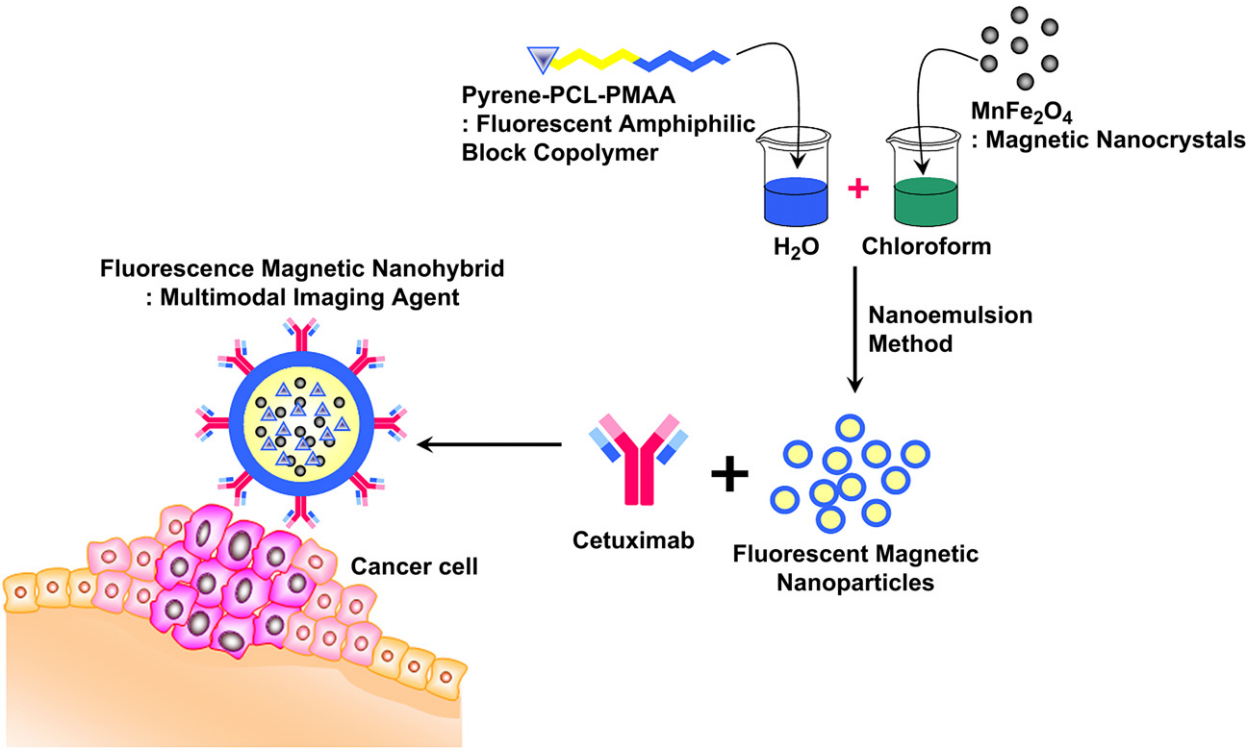

Fig. 1. The schematic illustration for preparation of fluorescence magnetic nanohybrids as multimodal imaging agents for cancer detection.

this amphiphilic block copolymer as a surfactant, the water-soluble MNCs were obtained by nano-emulsion method [13,14]. To assess the potential for a cancer-imaging probe with prepared fluorescent magnetic nanohybrids (FMNHs), the physico-chemical properties of the nanoparticles were fully investigated. As an EGFR targeting moiety, antibody (Cetuximab, CET) was further conjugated with the surface of FMNHs [16]. The cellular affinity and imaging efficacy of the antibody conjugated FMNHs (CET-FMNHs) have extensively been investigated using MR imaging and optical imager.

2. Materials and methods

2.1. Materials

The following materials were purchased from Sigma–Aldrich: iron (III) acetylacetonate, 1,2-hexadecanediol, dodecanoic acid, dodecylamine, benzyl ether, 1-ethyl-3-(3-dimethylaminopropyl)-carbodiimide, *N*-hydroxysuccinimide, *tert*-butyl methacrylate (*t*BMA), ϵ-caprolactone, trifluoroacetic acid (TFA), 1-pyrenebutyric acid, 1,3-dicyclohexylcarbodiimide (DCC), 4-dimethylaminopyridine (DMAP), copper (I) bromide (Cu(I)Br, 99.999%), *N*,*N*,*N*′,*N*′,*N*″-pentamethyldiethylenetriamine (PMDETA), stannous octoate ($Sn(Oct)_2$), anhydrous magnesium sulfate, 2-bromopropionyl bromide (BPB) and polyvinyl alcohol (PVA, M_w: 15–20 kDa). Tetrahydrofuran (THF) and toluene were distilled from Na/benzophenone under N_2 prior to use. Triethylamine (TEA), acetonitrile, and methylene chloride were dried and distilled over calcium hydride. All other chemicals and reagents were of analytical grade.

2.2. Synthesis of $MnFe_2O_4$ magnetic nanocrystals (MNCs)

The synthetic method for $MnFe_2O_4$ magnetic nanocrystals (MNCs) has been reported in a recent publication [1,13]. Briefly, 4 mmol iron (III) acetylacetonate, 2 mmol manganese (II) acetylacetonate, 20 mmol 1,2-hexadecanediol, 12 mmol dodecanoic acid, 12 mmol dodecylamine, and benzyl ether (50 mL) were mixed under nitrogen atmosphere. The mixture was preheated to 120 °C for 30 min and refluxed at 300 °C for 1 h. After the reactants were cooled to room temperature, the products were purified with an excess of pure ethanol. Approximately 12 nm of MNCs were synthesized after the seed-mediated growth [17].

2.3. Synthesis of pyrene-labeled poly(ϵ-caprolactone)-*b*-poly(methacrylic acid) (Py-PCL-*b*-PMAA)

Fluorescent amphiphilic block copolymers were synthesized using ring opening polymerization and atomic transfer radical polymerization [15]. Pyrene-labeled poly(ϵ-caprolactone)-*b*-poly(methacrylic acid) (Py-PCL-*b*-PMAA) was prepared by the following three-step synthetic routes: (i) synthesis of *R*-bromopropionyl-ö-hydroxy PCL (HO–PCL–Br), (ii) pyrene-labeled PCL-*b*-poly-(*tert*-butyl methacrylate) (Py-PCL-*b*-P*t*BMA), and (iii) deprotection of Py-PCL-*b*-P*t*BMA. For HO–PCL–Br, 2-hydroxyethyl 2′-bromopropionate (3.44 g, 0.0175 mol) in distilled toluene (90 mL) was dried azeotropically, and ϵ-caprolactone (30 g, 0.26 mol) was added into the hydroxyethyl 2′-bromopropionate solution. The polymerization was initiated by the addition of 0.14 g (0.35 mmol) of $Sn(Oct)_2$ at 120 °C, and the reaction mixture was stirred under nitrogen for 24 h. The HO–PCL–Br was isolated by precipitation from toluene into *n*-hexane (1 L) with a yield of 93%. To prepare pyrene-labeled PCL-*b*-poly(*tert*-butyl methacrylate) (Py-PCL-*b*-P*t*BMA), the HO–PCL–Br macroinitiator (3 g, 1.8 mmol) and Cu(I)Br (0.49 g, 7.1 mmol) were added to a flame-dried round-bottom flask. Toluene (10 mL) and *t*BMA were degassed by N_2 and added to the flask, and then PMDETA (1.48 g, 7.1 mmol) was introduced. The reaction temperature was maintained at 85 °C for 15 h. The block copolymers were purified by passing through the silica gel column and precipitation from THF into cold *n*-hexane. Pyrene was labeled at the terminal of the PCL block by DCC chemistry [18]. The block copolymers were denoted as Py-PCL-*b*-P*t*MBA. Finally, the deprotection of Py-PCL-*b*-P*t*BMA was performed by treating the block copolymers (3 g) with TFA (10 mL, 0.13 mol) in methylene chloride (10 mL). The aqueous solution was then dialyzed using a membrane (molecular weight cutoff (MWCO): 1000) for 24 h, followed by freeze-drying. The final block

copolymers were denoted as Py-PCL-*b*-PMAA (PPPs). Molecular weight (M_n) of PPPs was determined to be 4200 Da by using a gel permeation chromatography [15]. The chemical structure of PPPs was evaluated by ^{1}H-NMR; PCL protons, ($CO(CH_2)_4CH_2O$): 3.97 ppm and pyrenyl protons: 7.9–8.3 ppm, respectively. The resonance for the *tert*-butyl ester groups at 1.49 ppm completely disappeared after the hydrolysis [15].

2.4. Preparation of fluorescent magnetic nanohybrids (FMNHs)

Py-PCL-*b*-PMAA (PPPs) (50 mg) and MNCs (5 mg) were dissolved in 10 mL of dichloromethane. The organic phase was added to 20 mL of water. After mutual saturation of the organic and aqueous phase, the mixture was emulsified for 10 min with an ultrasonicator at 450 W [13]. After solvent evaporation, the products were purified with centrifugation (RPM: 20,000). The precipitated nanoparticles were redispersed in PBS (2 mL, pH 7.4, 10 mM). The size distribution and surface charge of FMNHs were analyzed by laser scattering (ELS-Z, Otsuka electronics). The saturation of magnetization was evaluated using vibrating-sample magnetometer (Lakeshore, model 7300). The weight quantity of magnetic nanocrystals in FMNHs was analyzed with a thermo-gravimetric analyzer (SDT-Q600, TA instrument). X-ray diffraction measurements of FMNHs were performed with a Rigaku D/max-RB (Tokyo, Japan) powder diffractometer and by image-plate photography using graphite-monochromatized Cu Kα radiation ($\lambda = 1.542$ Å). Data were collected from 20 to 70 degrees with a step size of 0.05 degree and step time of 5 s. Inductively Coupled Plasma Mass Spectroscopy (ICP-MS) was used for compositional analysis of FMNHs. ICP-MS analysis was carried out on a Perkin-Elmer Sciex Elan 6100 instrument (Wellesley, MA) using an argon plasma flame and dual detector mode.

2.5. Cetuximab conjugation with FMNHs (CET-FMNHs)

In order to prepare antibody conjugated FMNHs (CET-FMNHs), 1 mg of CET (Cetuximab) was dissolved in 400 μL of PBS and mixed with 100 μL of FMNHs solution (10 mg/mL). *N*-hydroxysuccinimide (2.0 mM) and 1-ethyl-3-(3-dimethylaminopropyl)-carbodiimide (2.0 mM) were added to the previous solution. After 4 h, CET-FMNHs were purified with a Sephacryl S-300 column (Amersham Biosciences) and ultra centrifugal filter (Amicon Ultra). A BCA kit was used to measure the amount of CET conjugated to FMNHs surface. The human IgG-conjugated FMNHs (IgG-FMNHs) as a control were synthesized in the manner described above.

2.6. Cell affinity test

The cancer cell affinity of CET-FMNHs was investigated using flow cytometry and epi-fluorescence microscopy. Target cancer cells (A431, MCF cells, 1×10^6 cells/mL) were incubated and treated with CET-FMNHs for 30 min. The solution was washed three times with 0.2% fetal bovine serum (FBS) and 0.02% NaN_3 in PBS. The samples were resuspended in 400 μL of 4% paraformaldehyde and incubated with FITC (fluorescein isothiocyanate)-labeled goat anti-human IgG for 45 min at 4 °C in the dark room [18]. Then the cells were suspended in 500 μL of PBS and stored at 4 °C. FACScalibur (Beckton-Dickinson, Mansfield, MA) was used to monitor the cell-associated fluorescence. Data were collected and analyzed from 10,000 gated events.

2.7. In vitro imaging procedure

All MR imaging experiments were performed with a 1.5-T clinical MRI instrument with a micro-47 surface coil (Intera; Philips Medical Systems, Best). For T2-weighted MR imaging of *in vitro* cells at 1.5 T, the following parameters were adopted: point resolution: 156×156 μm, section thickness of 0.6 mm, TE = 60 ms, TR = 4000 ms and number of acquisitions = 1. For T2 mapping of *in vitro* cells, the following parameters were adopted: point resolution of 156×156 μm, section thickness of 0.6 mm, TE = 20, 40, 60, 80, 100, 120, 140, 160 ms, TR = 4000 ms and number of acquisitions = 2. R2 was defined as 1/T2 s^{-1}. Fluorescence intensities of FMNHs treated cells were investigated using Optical imager (eXplore Optix MX, GE Healthcare).

3. Results and discussion

Magnetic nanocrystals (MNCs) as MR imaging probes were synthesized using the seed-mediated growth method at high temperature. The morphology and monodispersity of MNCs were evaluated by TEM, as shown in Fig. 2a. The size of MNCs synthesized in oil phase was ~12 nm. To fabricate water-soluble MNCs, the surface of the MNCs was modified with synthesized amphiphilic block copolymers. The PCL-*b*-PMAA as amphiphilic block copolymer was synthesized and then pyrene was conjugated at the terminal hydrophobic part of PCL-*b*-PMAA for optical imaging.

Water-soluble, fluorescent magnetic nanohybrids (FMNHs) using pyrene-labeled PCL-*b*-PMAA (PPPs) and MNCs were prepared by a nano-emulsion method. FMNHs capped with hydrophilic PMAA chains could be soluble in the aqueous phase. The spherical shape of FMNHs was verified with TEM (Fig. 2b). The hydrodynamic radius of FMNHs was 112.7 ± 3.2 nm as determined by laser scattering. The surface charge of FMNHs presented negative value and the zeta potential was -43.5 ± 4.6 mV due to the carboxyl group of PMAA chains. In addition, the water-soluble FMNHs exhibited high

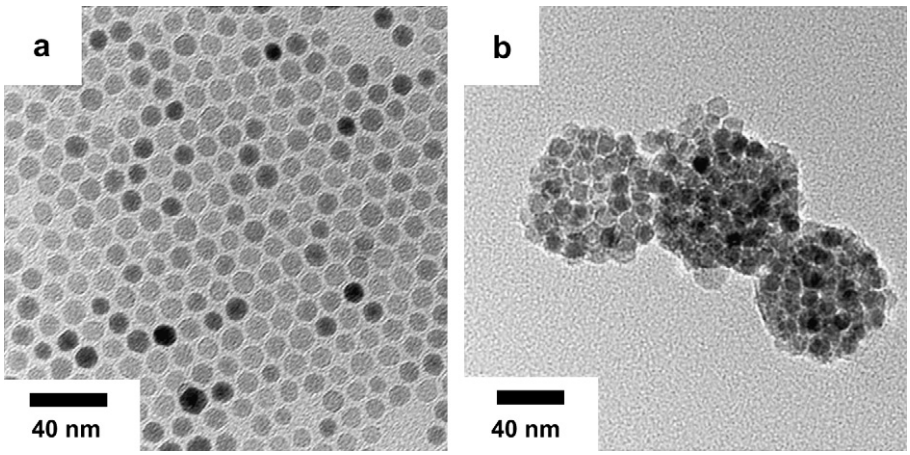

Fig. 2. TEM images of (a) MNCs and (b) FMNHs.

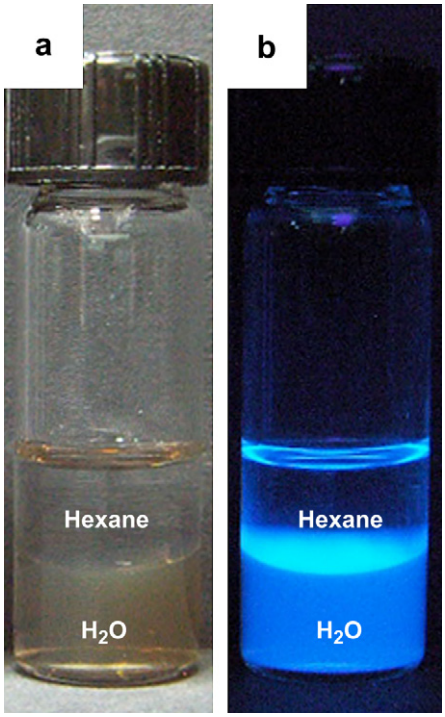

Fig. 3. Solubility test of FMNHs. (a) FMNHs in H_2O under visible light. (b) Luminescence of FMNHs in H_2O by UV lamp.

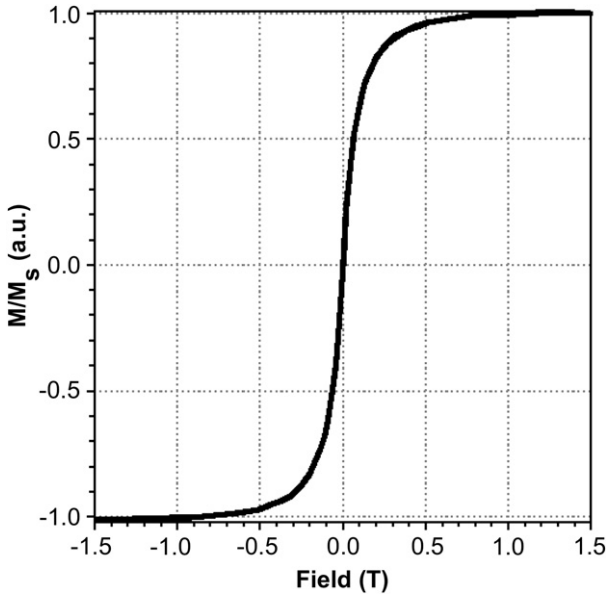

Fig. 5. Magnetic hysteresis loop of FMNHs using vibration sample magnetometer.

colloidal stability in the aqueous phase and the fluorescent property under UV light (365 nm) due to subsistence of pyrene in FMNHs (Fig. 3).

FT-IR spectrum of FMNHs was compared with that of PPPs (Fig. 4). Carboxyl group (−COOH) of PMAA chain and ester group (−COO) of PCL chain were verified at 1725 cm^{-1} due to C═O bond, and O−H stretch of PMAA chain was detected at 3000−3300 cm^{-1}. Also, the characteristic peak of the Fe−O bond was observed at 585 cm^{-1} due to the presence of MNCs in FMNHs.

The hysteresis loop of FMNHs was obtained by using a vibration sample magnetometer at 300 K (Fig. 5). FMNHs exhibited a superparamagnetic behavior without magnetic hysteresis, and the saturation of magnetization (M_s) at 1.5 T of FMNHs was 52.5 emu/g. Because of the polymeric components of FMNHs, the M_s of FMNHs was smaller than the M_s of pure MNCs (87 emu/g). The ratio of magnetic components and polymeric compounds in FMNHs was measured by thermo-gravimetric analyzer. When the organic components were removed at 210−270 °C, the quantity of inorganic residue (MNCs in FMNHs) was 33.1 wt%. In addition, the crystallinity of MNCs was still maintained after formation of FMNHs (Fig. 4b).

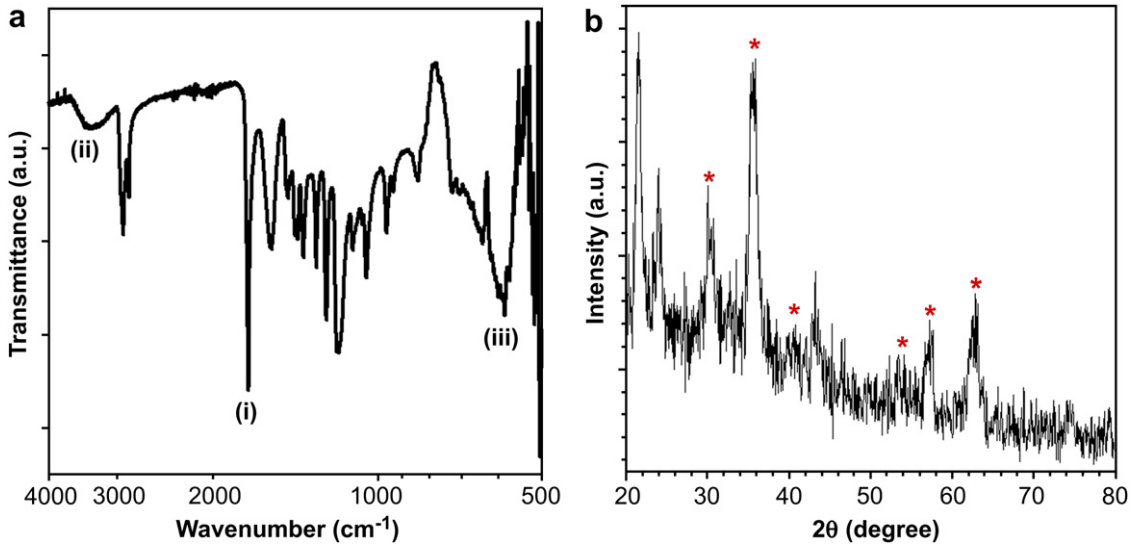

Fig. 4. (a) FT-IR analysis of FMNHs: (i) carboxyl group of PMAA chain and ester group of PCL chain, (ii) hydroxyl group stretch of PMMA and (iii) Fe−O bond of MNCs. (b) X-ray diffraction pattern of FMNHs. The peaks of the $MnFe_2O_4$ nanocrystal structure are marked with asterisks (*).

The magnetic sensitivity under magnetic field was investigated using MR imaging. The spin–spin relaxation time (T2) weighted spin–echo MR images of FMNHs significantly increased with increasing concentration of Fe + Mn (Fig. 6a). Similarly, the relaxivity (R2) of FMNHs linearly increased under these conditions. Interestingly, despite smaller M_s value, the relaxivity coefficient of FMNHs by magnetic field was 404 $mM^{-1} s^{-1}$, which was higher than the values of single MNCs, due to clustering effect of magnetic nanoparticles [1,19].

The prepared FMNHs suspension emitted the fluorescent blue light under illumination of UV light (330–385 nm) (Fig. 7a). When the permanent magnet (Nd–Fe–B, 0.35 T) was placed nearby, FMNHs moved toward the magnet and gathered at the sidewall of microchannel within 1 min (Fig. 7c).

To evaluate the biocompatibility of FMNHs as bio-imaging probes, we investigated the cytotoxicity of FMNHs using the MTT assay. FMNHs exhibited low cytotoxicity towards MCF7 and A431 cells even at high concentrations (100 μg/mL) (Fig. 8).

The cancer cell targeting efficacy of CET-FMNHs as multimodal imaging probes was investigated. Cell affinity against A431 cells highly expressing EGFR cancer markers were compared with the one against MCF7 cells expressing low

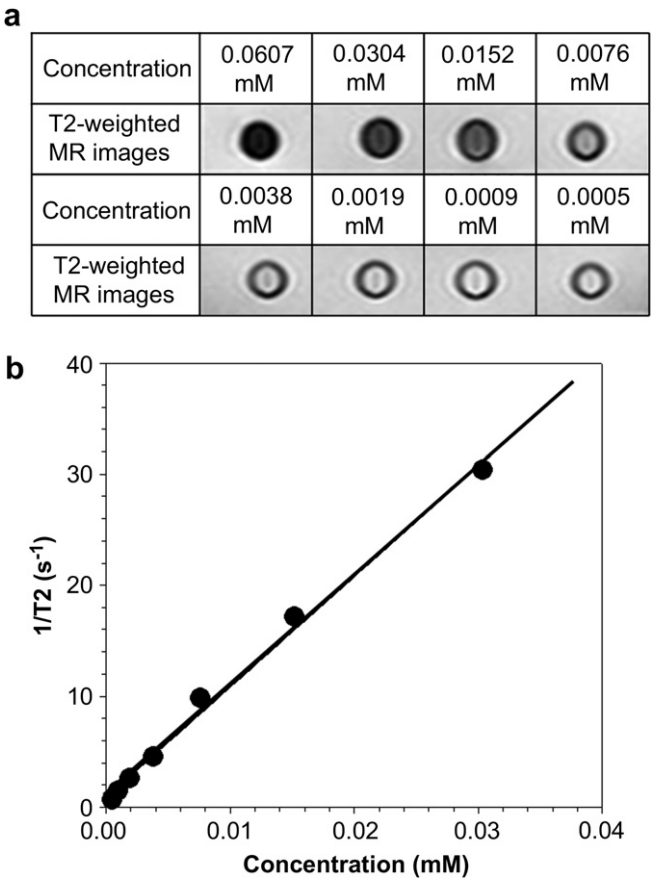

Fig. 6. (a) T2-weighted MR images of FMNHs in aqueous solution. (b) Graph of R2 relaxivity against the concentration of FMNHs.

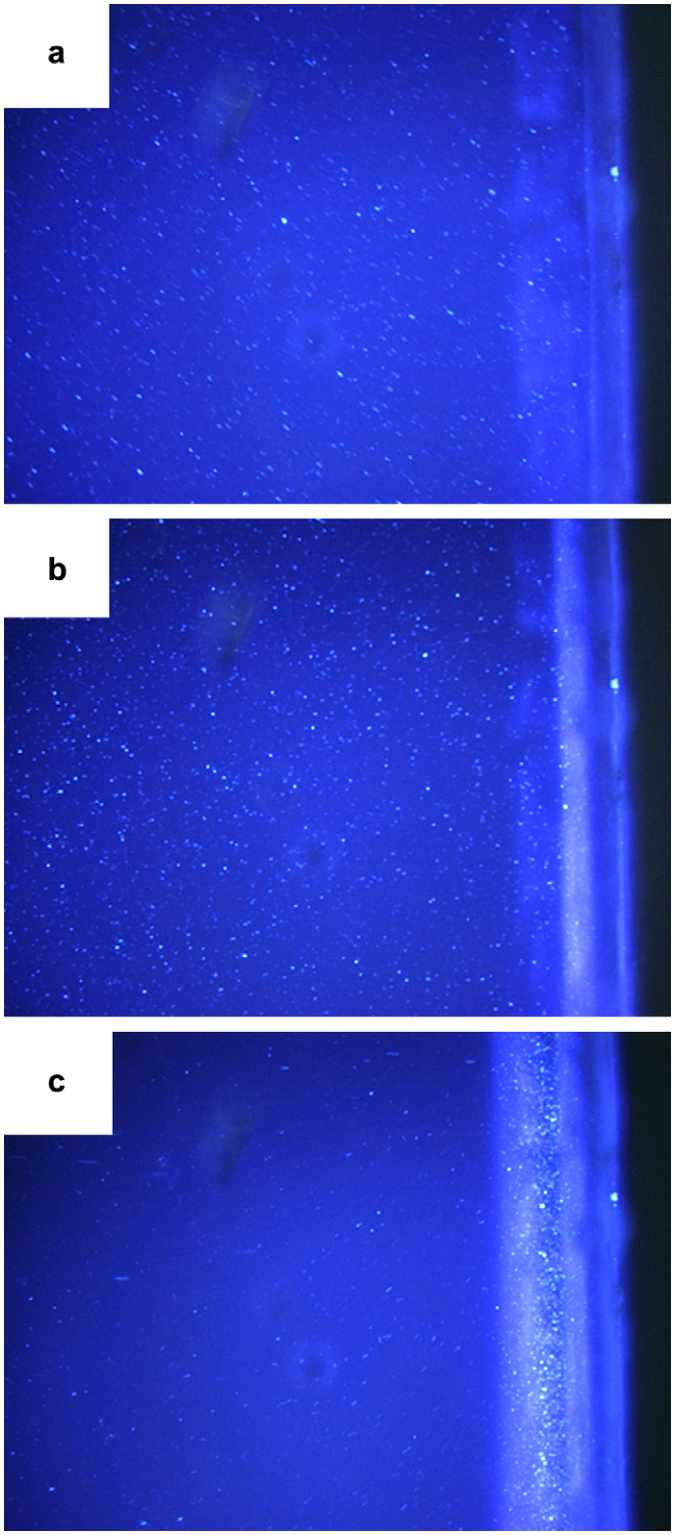

Fig. 7. Fluorescence microscopic images of FMNHs under magnetic field (×400). Nd–Fe–B magnet is located at right-side of the microchannel. FMNHs were gathered at right-side of microchannel from (a) to (c).

levels of the cancer markers. In Fig. 9a, MCF7 cells incubated with IgG-FMNHs or CET-FMNHs presented minimal shift of fluorescence intensity (FI) and the FI was similar with non-treated cells. In contrast, A431 cells incubated with CET-

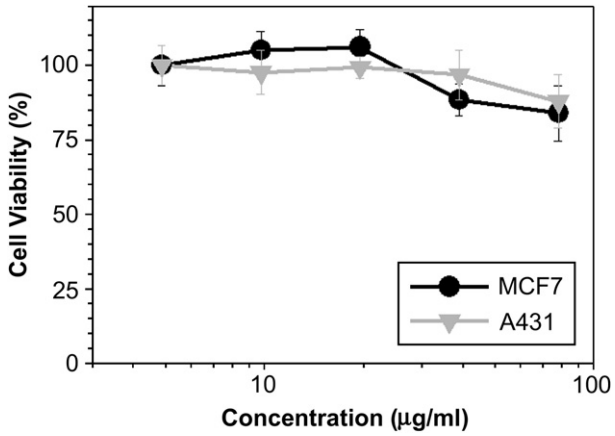

Fig. 8. Cell viability test of A431 (a, b) and MCF7 (c, d) cells incubated with CET-FMNHs.

FMNHs demonstrated a higher relative FI compared with IgG-FMNHs treated cells (Fig. 9b), and the relative intensity was 43.9 times higher than that of non-treated cells (Fig. 9c). Furthermore, the cellular binding efficiencies of CET-FMNHs for the cancer cell lines were visualized using a fluorescence microscope. In case of A431 cells incubated with CET-FMNHs (Fig. 10a), a green color appeared due to FITC-labeled goat anti-human IgG conjugated with CET by blue excitation filter (460–490 nm). However, MCF7 cells treated with CET-FMNHs presented faint green color due to deficiency of EGFR (Fig. 10c). In the UV region (330–360 nm), A431 cells incubated with CET-FMNHs should emit the blue light because of pyrene in FMNHs; however, the cells emitted the green light (Fig. 10b). This can be explained due to overlapping the emission wavelength of pyrene in FMNHs the excitation wavelength of FITC (Fig. 10e) and resulting in occurrence of fluorescence resonance electron transfer (FRET) phenomenon. The emitted light of pyrene under UV light embodied an excitation of FITC. Therefore, green color on the A431 cells incubated with CET-FMNHs was detected by fluorescence microscope image. Moreover, MCF7 cells incubated with CET-FMNHs exhibited a faint fluorescence light because of a low expressed amount of EGFR, indicating acceptable specific cellular binding efficiency of CET-FMNHs. FACS analysis and fluorescence microscopy demonstrated that CET-FMNHs successfully bound target cancer cells.

The T2-weighted MR images of cancer cell lines using CET-FMNHs were investigated for evaluation of the potential MR contrast agents (Fig. 11). The MR image of A431 cells incubated with CET-FMNHs exhibited a black color and MCF7 cells incubated with CET-FMNHs presented gray due to low levels of the cancer markers (Fig. 11a). Furthermore, the color maps for the T2-weighted MR images indicated similar results. Except for the A431 cells incubated with CET-FMNHs, other cells demonstrated a blue or green color (Fig. 11b). The changes of $\Delta R2/R2_{NT}$ for the CET-FMNHs treated A431 cells compared to the non-treated cells were ~83.16%, as shown in Fig. 11c. These results demonstrated the efficient targeted delivery of CET-FMNHs for the EGFR of cancer cells.

To verify the CET-FMNHs as multimodal imaging probes, we further investigated the optical images of target cells using optical imager. The tested cells for MR imaging were irradiated using blue laser (488 nm) and the emitted light from

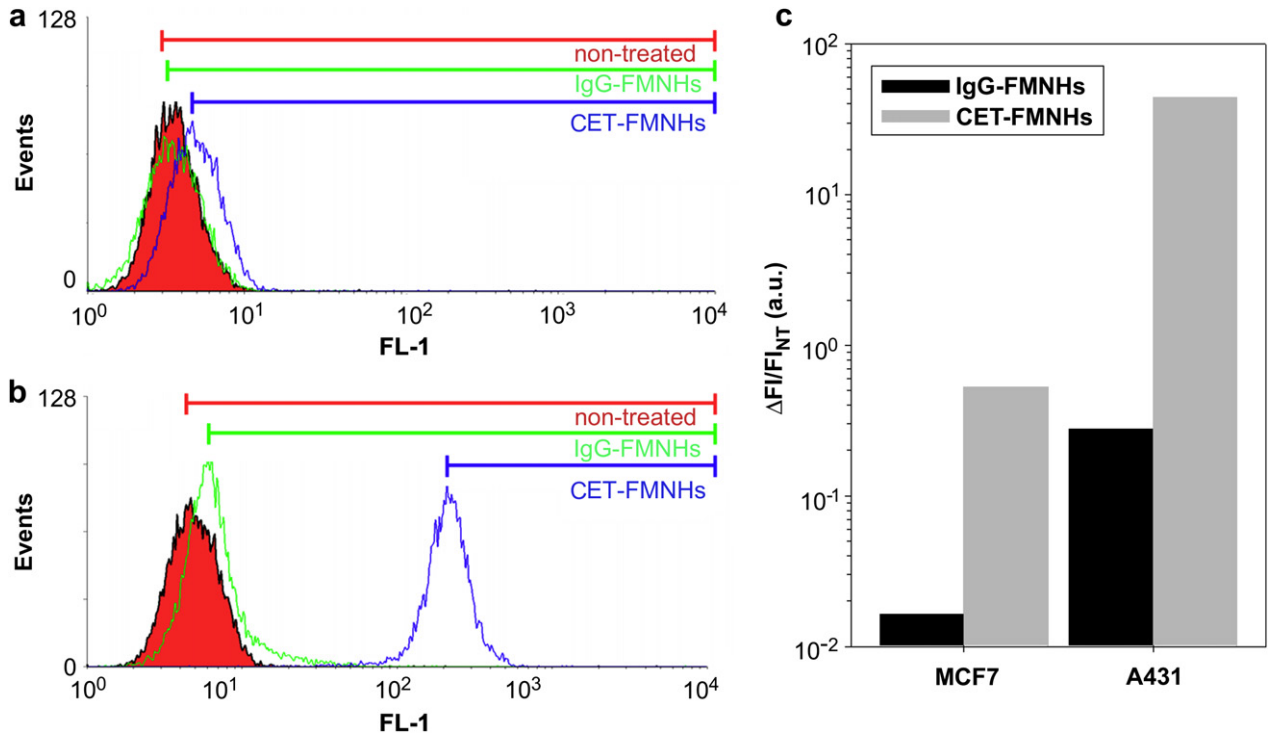

Fig. 9. FACS analysis of (a) A431 and (b) MCF7 cells; red: non-treated cells, green: IgG-FMNHs treated cells and blue: CET-FMNHs. (c) Relative fluorescence intensity (ΔFI/FINT; FI: fluorescence intensity and NT: non-treated) via FACS analysis.

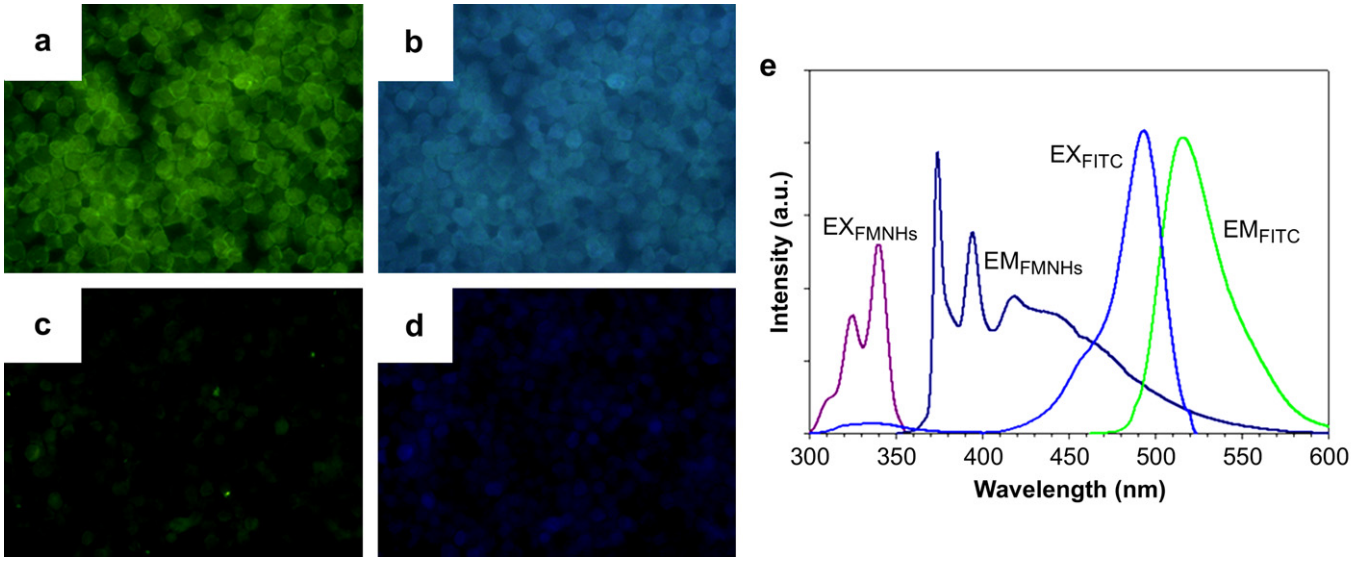

Fig. 10. Fluorescence microscopy images of (a, b) A431 and (c, d) MCF7 cells incubated with CET-FMNHs; (a, c) green filter and (b, d) blue filter. (e) Fluorescence intensity graph of FMNHs (purple: excitation, indigo blue: emission) and FITC (blue: excitation, green: emission).

interrogate cells was observed. The optical imaging results were analogous with MR imaging results (Fig. 12a). A431 cells treated with CET-FMNHs exhibited a strong fluorescence light and the relative FI when compare with the non-treated cells ($\Delta FI/FI_{NT}$) was 1000.32% (Fig. 12b). On the other hand, A431 cells treated with IgG-FMNHs and MCF7 cells emitted a faint fluorescence light and $\Delta FI/FI_{NT}$ was low. The MR and optical imaging results clearly show the manifest enormous potential of CET-FMNHs as multimodal imaging agents for cancer detection.

4. Conclusions

We successfully synthesized Cetuximab conjugated fluorescent magnetic nanohybrids (CET-FMNHs) for detection of cancer using MR and optical imaging. The well tailored spherical

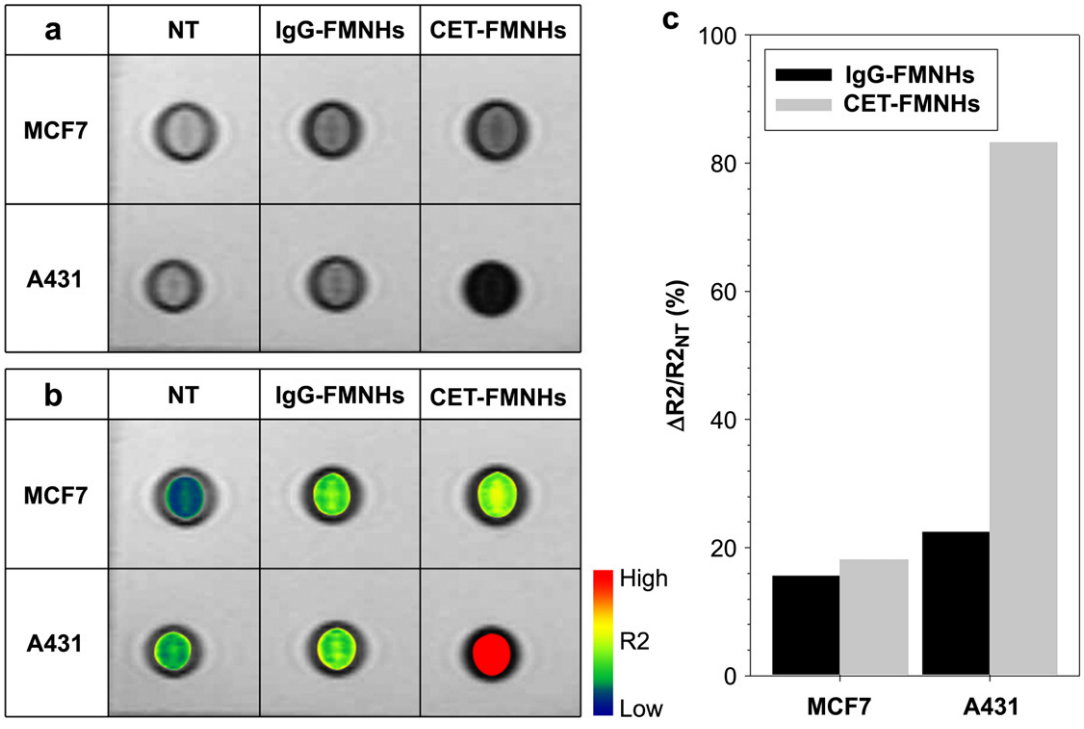

Fig. 11. (a) T2-weighted MR images and (b) their color maps of A431 and MCF7 cells treated with CET-FMNHs and IgG-MPPs. (c) ΔR2/R2NT graph for A431 and MCF7 cells. NT: non-treated.

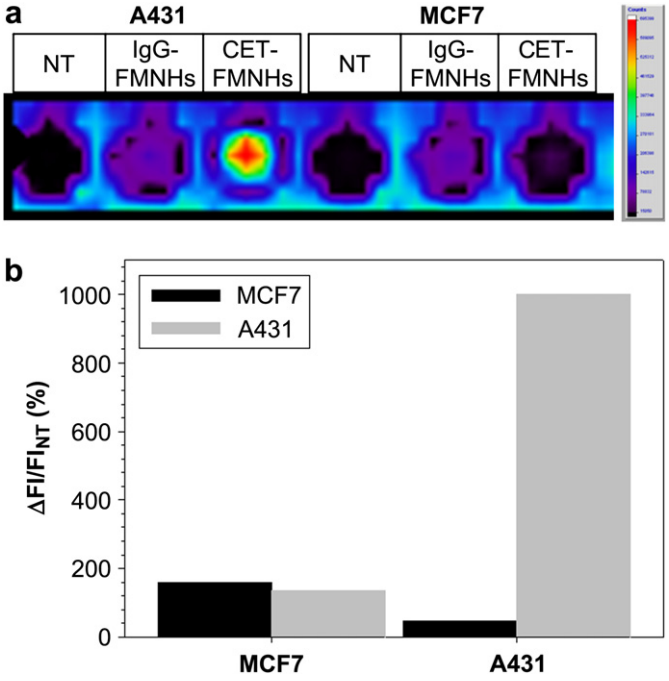

Fig. 12. (a) Optical imaging of A431 and MCF7 cells incubated with IgG-FMNHs and CET-FMNHs, respectively. (b) Relative optical fluorescence intensity (ΔFI/FINT; FI: fluorescence intensity).

FMNHs were prepared by a nano-emulsion method from magnetic nanocrystals and pyrene-labeled PCL-*b*-PMAA as a surfactant. Cytotoxicity test demonstrated that the prepared FMNHs possessed a suitable property for biomedical application. Antibody conjugated fluorescent magnetic nanohybrids, CET-FMNHs exhibited excellent ability as agents for MR and fluorescence optical imaging of cancer cell lines, respectively. These fluorescent magnetic nanohybrids as multimodal imaging agents can be applied for detection of early state of cancer.

Acknowledgments

This work was supported by KOSEF through National Core Research Center for Nanomedical Technology (M107550 20001-07N5502-00110, R15-2004-024-00000-0 and R01-2006-000-10023-0), the National R&D Program for Cancer Control, Ministry of Health & Welfare, Republic of Korea (0620190-1).

Appendix A. Supplementary material

Supplementary material for this article can be found, in the online version, at doi:10.1016/j.biomaterials.2007.12.036

References

[1] Lee J, Huh YM, Jun Y, Seo J, Jang J, Song H, et al. Artificially engineered magnetic nanoparticles for ultra-sensitive molecular imaging. Nat Med 2007;13:95–9.
[2] Huh YM, Jun Y, Song H, Kim S, Choi J, Lee J, et al. In vivo magnetic resonance detection of cancer by using multifunctional magnetic nanocrystals. J Am Chem Soc 2005;127:12387–91.
[3] Na HB, Lee JH, An K, Park YI, Park M, Lee IS, et al. Development of a T1 contrast agent for magnetic resonance imaging using MnO nanoparticles. Angew Chem Int Ed 2007;46:5397–401.
[4] Song H, Choi J, Huh YM, Kim S, Jun W, Suh JS, et al. Surface modulation of magnetic nanocrystals in the development of highly efficient magnetic resonance probes for intracellular labeling. J Am Chem Soc 2005;127:9992–3.
[5] Schneider T, Moore LR, Jing Y, Haam S, Williams PS, Fleischman AJ, et al. Continuous flow magnetic cell fractionation based on antigen expression level. J Biochem Biophys Methods 2006;68:1–21.
[6] Graham DL, Ferreira HA, Felicianoa N, Freitas PP, Clarke LA, Amaral MD. Magnetic field-assisted DNA hybridisation and simultaneous detection using micron-sized spin-valve sensors and magnetic nanoparticles. Sens Actuators B Chem 2005;107:936–44.
[7] Weissleder R, Moore A, Mahmood U, Bhorade R, Benveniste H, Chiocca EA, et al. In vivo magnetic resonance imaging of transgene expression. Nat Med 2000;6:351–4.
[8] Tanaka S, Ota H, Kondo Y, Tamaki Y, Kobayashi S, Noguchi S. Detection of magnetic nanoparticles in lymph nodes of rat by high Tc SQUID. IEEE Trans Appl Supercond 2003;13:377–80.
[9] Jun Y, Huh YH, Choi J, Lee J, Song H, Kim S, et al. Nanoscale size effect of magnetic nanocrystals and their utilization for cancer diagnosis via magnetic resonance imaging. J Am Chem Soc 2005;127:5732–3.
[10] Albrecht K, Greindl M, Kremser C, Wolf C, Debbage P, Bernkop-Schnürch A. Comparative in vivo mucoadhesion studies of thiomer formulations using magnetic resonance imaging and fluorescence detection. J Control Release 2006;115:78–84.
[11] Bertorelle F, Wilhelm C, Roger J, Gazeau F, Menager C, Cabuil V. Fluorescence-modified superparamagnetic nanoparticles: intracellular uptake and use in cellular imaging. Langmuir 2006;22:5385–91.
[12] Mulder W, Koole R, Brandwijk RJ, Storm G, Chin P, Strijkers GJ, et al. Quantum dots with a paramagnetic coating as a bimodal molecular imaging probe. Nano Lett 2006;6:1–6.
[13] Yang J, Lee CH, Park J, Seo S, Lim EK, Song YJ, et al. Antibody conjugated magnetic PLGA nanoparticles for diagnosis and treatment of breast cancer. J Mater Chem 2007;17:2695–9.
[14] Michalet X, Pinaud FF, Bentolila LA, Tsay JM, Doose S, Li JJ, et al. Quantum dots for live cells, in vivo imaging, and diagnostics. Science 2005;307:538–44.
[15] Lee SC, Lee HJ. pH-Controlled polymer-mediated assembly of polymer micelle nanoparticles. Langmuir 2007;23:488–95.
[16] Harding J, Burtness B. Cetuximab: an epidermal growth factor receptor. chimeric human-murine monoclonal antibody. Drugs Today 2005;41:107.
[17] Sun S, Zeng H, Robinson DB, Raoux S, Rice PM, Wang SX, et al. Monodisperse MFe_2O_4 (M = Fe, Co, Mn) nanoparticles. J Am Chem Soc 2004;126:273–9.
[18] Hermanson GT. Bioconjugate technique. USA: Academic Press; 1996.
[19] Berret J, Schonbeck N, Gazeau F, Kharrat D, Sandre O, Vacher A, et al. Controlled clustering of superparamagnetic nanoparticles using block copolymers: design of new contrast agents for magnetic resonance imaging. J Am Chem Soc 2006;128:1755–61.